

Highlights

HiRes-FusedMIM: A High-Resolution RGB-DSM Pre-trained Model for Building-Level Remote Sensing Applications

Guneet Mutreja, Philipp Schuegraf, Ksenia Bittner

- A unique dataset of over 368k paired RGB-DSM images at 0.2-0.5 m resolution is curated from various sources across Europe to train a multimodal pre-trained model- HiRes-FusedMIM.
- A novel dual encoder SimMIM architecture facilitating joint representation learning is developed.
- Demonstrated the effectiveness of HiRes-FusedMIM on a diverse set of building-related tasks, including classification, semantic segmentation, and instance segmentation.

HiRes-FusedMIM: A High-Resolution RGB-DSM Pre-trained Model for Building-Level Remote Sensing Applications

Guneet Mutreja^a, Philipp Schuegraf^a, Ksenia Bittner^a

^a*German Aerospace Center (DLR), Münchener Straße
20, Weßling, 82234, Bavaria, Germany*

Abstract

Recent advances in self-supervised learning have led to the development of foundation models that have significantly advanced performance in various computer vision tasks. However, despite their potential, these models often overlook the crucial role of high-resolution digital surface models (DSMs) in understanding urban environments, particularly for building-level analysis, which is essential for applications like digital twins. To address this gap, we introduce HiRes-FusedMIM, a novel pre-trained model specifically designed to leverage the rich information contained within high-resolution RGB and DSM data. HiRes-FusedMIM utilizes a dual-encoder simple masked image modeling (SimMIM) architecture with a multi-objective loss function that combines reconstruction and contrastive objectives, enabling it to learn powerful, joint representations from both modalities. We conducted a comprehensive evaluation of HiRes-FusedMIM on a diverse set of downstream tasks, including classification, semantic segmentation, and instance segmentation. Our results demonstrate that: 1) HiRes-FusedMIM outperforms previous state-of-the-art geospatial methods on several building-related datasets, including WHU Aerial and LoveDA, demonstrating its effectiveness in capturing and leveraging fine-grained building information; 2) Incorporating DSMs during pre-training consistently improves performance compared to using RGB data alone, highlighting the value of elevation information for building-level analysis; 3) The dual-encoder architecture of HiRes-FusedMIM, with separate encoders for RGB and DSM data, significantly outperforms a single-encoder model on the Vaihingen segmentation task, indicating the benefits of learning specialized representations for each modality. To facilitate further research and applications in this direction, we will publicly release the

trained model weights.

Keywords: Masked Image Modeling (MIM), Multi-Modal Learning, Digital Surface Models (DSMs), Self-Supervised Learning, Foundation Models

PACS: 0000, 1111

2000 MSC: 0000, 1111

1. Introduction

Accurate and up-to-date information about buildings is crucial for a wide range of applications, from urban planning and disaster response to the creation of digital twins. Detailed 3D building models, in particular, are essential for simulating urban environments, assessing risks, and optimizing infrastructure management.

High-resolution imagery, particularly the fusion of RGB and digital surface models (DSMs), plays a crucial role in extracting detailed building information. While RGB data captures spectral characteristics of the surface of the Earth, DSMs provide critical elevation information, enabling the derivation of building heights and 3D structures. In recent years, foundation models, pre-trained on massive datasets using self-supervised learning, have revolutionized computer vision and shown great promise in remote sensing [8, 35, 6, 21]. These models learn general-purpose visual representations that can be adapted to various downstream tasks, including those requiring precise building information.

Despite the advantages of foundation models and the importance of high-resolution DSMs, existing approaches in remote sensing often fall short in fully leveraging the potential of this combination. This gap stems primarily from the limited availability of large-scale, high-resolution RGB-DSM datasets and the inherent challenges in effectively fusing these modalities during pre-training. Models predominantly trained on open-source data like Sentinel-2 imagery (10 m resolution) [21] often struggle to generalize well to tasks requiring finer details [34]. While some efforts have incorporated high-resolution RGB data [26], the development of pre-trained models that effectively leverage high-resolution DSMs, especially for building-level analysis, remains a significant area for explorations.

This paper addresses this gap by introducing HiRES-FUSEDMIM, a novel pre-trained model specifically designed for building-level remote sensing applications. HiRes-FusedMIM leverages a unique and extensive dataset of

paired RGB-DSM imagery at 0.2-0.5m resolution, carefully curated from various sources. The model utilizes a dual encoder simple masked image modeling (SimMIM) architecture [40] with a multi-objective loss function that combines both reconstruction and contrastive objectives. We demonstrate the effectiveness of this approach on a diverse range of downstream tasks, including classification, semantic segmentation, and instance segmentation, showing its superior performance in capturing and leveraging high-resolution, multi-modal information for detailed building analysis.

The paper is organized as follows: Section 2 reviews related work on importance of DSMs, self-supervised learning, and foundation models in remote sensing. Section 3 details the HiRes-FusedMIM methodology, including the dataset, model architecture, and pre-training process. Section 4 presents the experimental results, comparing our approach to relevant baselines and state-of-the-art methods. Section 5 presents a series of ablation studies analyzing the impact of different model components. Finally, Section 6 discusses the implications of our findings and outlines future research directions.

2. Related work

This section provides a comprehensive review of existing research relevant to the development and applications of HiRes-FusedMIM. We first discuss the significance of DSMs in remote sensing, followed by a discussion of recent advancements in self-supervised learning and foundation models for remote sensing. Finally, we highlight the motivation and contributions of our research, emphasizing the novelty of our approach.

2.1. The Importance of DSMs in Remote Sensing

DSMs are essential data sources in remote sensing, providing crucial elevation information about the surface of the Earth and all objects upon it. Unlike digital terrain models (DTMs), which represent the bare earth, DSMs capture the heights of buildings, vegetation, trees, and other structures. This detailed elevation data is essential for a wide range of applications, including:

- **Urban Planning and Analysis:** DSMs are used to analyze urban morphology, model urban growth, assess urban density, and aid in infrastructure planning and management.
- **Forestry and Vegetation Management:** DSMs are used to estimate forest canopy heights, analyze forest structure, monitor deforestation, and assess biomass.

- **Disaster Management:** DSMs play a vital role in flood modeling, landslide risk assessment, and damage assessment after natural disasters.
- **3D Building Reconstruction:** DSMs provide the height information necessary to create realistic 3D building models, which are essential for applications like urban planning, virtual city modeling, and digital twins.

The recent advancements in deep learning have significantly improved the utilization of DSMs in remote sensing, enabling the development of more automated and accurate methods for various tasks. Deep learning models, particularly convolutional neural networks (CNNs), have demonstrated success in:

- **Semantic Segmentation of DSMs:** CNNs can effectively classify DSM pixels into different categories, such as buildings, vegetation, and water bodies, enabling the automatic extraction of features with high accuracy [4, 5, 30, 33].
- **Joint Learning from RGB and DSM Data:** By combining RGB and DSM data, deep learning models can learn richer representations, leveraging both spectral and elevation information to achieve superior performance in tasks like land cover classification, object detection, and semantic segmentation [5, 14, 32, 31].
- **Generating levels of detail (LoD)2-Level Building Models:** Recent studies have demonstrated the potential of deep learning in achieving LoD2-level 3D building reconstruction by extracting roof planes and other detailed features from DSMs [14, 41, 31, 15].

This progress in deep learning, combined with the increasing availability of high-resolution DSM data, has opened new possibilities for extracting valuable information from remote sensing data and addressing complex challenges in various domains.

2.2. Self-Supervised Learning and Foundation Models in Remote Sensing

The field of remote sensing has been significantly impacted by the recent advancements in self-supervised learning (SSL) and foundation models. SSL enables models to learn valuable representations from unlabeled data, reducing the reliance on costly and often limited labeled datasets [13]. This

capability is particularly beneficial in remote sensing, where obtaining large-scale, high-quality labeled data is challenging.

Foundation models, typically large-scale neural networks pre-trained on massive datasets using SSL objectives, have emerged as a powerful paradigm for various computer vision tasks. These models learn general-purpose visual representations that can be effectively adapted to a wide range of downstream tasks, often achieving state-of-the-art performance with minimal fine-tuning.

In remote sensing, foundation models have demonstrated significant promise in tasks such as scene classification, object detection, and semantic segmentation. For instance, Cong et al. [8] developed a transformer-based model pre-trained on temporal and multi-spectral satellite imagery using a masked autoencoder (MAE) approach. This model effectively captures temporal and spectral information, enhancing performance in downstream tasks. Similarly, Sun et al. [35] utilizes an autoencoder architecture pre-trained on a large collection of very high-resolution RGB images, specifically designed to address the challenges of dense, small object detection in remote sensing data.

Another notable example is the work by Mendieta et al. [26], which employs a continual pre-training paradigm and a multi-objective loss function to learn robust representations. Jakubik et al. [21] proposed a transformer-based model pre-trained on a large-scale Harmonized Landsat-Sentinel 2 (HLS) dataset, demonstrating its effectiveness in real-world applications like flood mapping and crop segmentation.

Furthermore, Cha et al. [6] explored the scaling of model parameters in remote sensing foundation models. The research shows promising results on tasks such as rotated object detection and semantic segmentation, indicating that scaling up model size can capture more complex patterns inherent in remote sensing data.

These models demonstrate the power of SSL pre-training in capturing meaningful patterns and features from remote sensing data. However, a critical gap remains in fully leveraging the potential of high-resolution DSM data within this pre-training paradigm, especially for tasks focused on detailed building-level analysis.

2.3. Bridging the Gap: Towards High-Resolution, Multi-Modal Foundation Models for Building Analysis

Despite the promising advancements in foundation models, their application to building-level remote sensing tasks remains limited. Existing models primarily rely on medium-resolution satellite data like Sentinel-2 [8, 21, 3] or

focus solely on RGB information [26, 28], neglecting the valuable elevation data provided by high-resolution DSMs.

While some multi-modal models have been proposed, they haven't effectively addressed the challenges of high-resolution DSMs and their potential for building analysis. For example:

- DeCUR [38]: While demonstrating promising results on RGB-DEM fusion for semantic segmentation, their experiments used a smaller dataset data compared to the large-scale data employed in our research.
- MultiMAE [1]: This approach extends the MAE framework to accept multiple modalities, but its performance when integrating high-resolution DSM data with RGB remains unexplored, especially for building-related tasks.

Although other multi-modal models have been pre-trained, such as Han et al. [17] and Guo et al. [16], they do not explicitly emphasize the use of DSMs for building-level tasks. This underutilization of high-resolution DSMs persists despite their proven value in extracting building heights, reconstructing roof shapes, and generating detailed 3D building models [14, 36].

Our research seeks to address this gap by developing HiRes-FusedMIM, a pre-trained model explicitly designed to leverage high-resolution RGB-DSM data for building-level analysis. We will demonstrate how effectively integrating these modalities during pre-training leads to superior performance in downstream tasks that require fine-grained building information.

2.4. Contributions

This paper addresses this critical gap of underutilization of DSMs by introducing HiRes-FusedMIM, a novel pre-trained model designed explicitly to leverage high-resolution RGB-DSM data for pre-training, with a specific focus on building-related remote sensing applications. Our key contributions include:

- Curating a Large-Scale, High-Resolution, Paired RGB-DSM Dataset: We curated a unique dataset of over 368k paired RGB and DSM images at 0.2-0.5 m resolution, meticulously collected from various sources across Europe. This dataset, while not publicly shared due to licensing restrictions, serves as a vital foundation for training our model and highlights the need for more publicly available high-resolution, multi-modal datasets in the remote sensing community.

- **Effective Multi-Modal Fusion with a Dual Encoder SimMIM Architecture:** HiRes-FusedMIM utilizes a dual encoder SimMIM architecture [40] with separate encoders for RGB and DSM data. This architecture facilitates efficient joint representation learning, capturing both modality-specific and cross-modal features. A contrastive loss (InfoNCE) [27] is introduced between the encoder outputs to explicitly encourage the alignment of RGB and DSM representations, further enhancing the ability of the model to learn from both modalities.
- **Superior Performance on Building-Level Downstream Tasks:** We demonstrate the effectiveness of HiRes-FusedMIM on a diverse set of building-related tasks, including classification, semantic segmentation, and instance segmentation. Our experiments showcase superior performance compared to models trained on lower-resolution or single-modality data, validating the benefits of incorporating high-resolution DSMs in the pre-training process. To facilitate further research in this direction, we will publicly share the trained model weights.

3. Methodology

3.1. Pre-Training Dataset – A High-Resolution RGB-DSM Collection

A critical component of HiRes-FusedMIM is the creation of a unique, large-scale dataset of paired RGB and DSM imagery, carefully curated to facilitate the learning of representations optimized for building-level analysis. Addressing the limited availability of publicly accessible high-resolution DSM data, we combined multiple sources to construct this dataset. A major chunk of the data was sourced from open-source geoportals provided by local governments across Europe. We targeted cities that offer aerial imagery and corresponding DSMs at high resolutions (20 cm - 50 cm), striving to encompass a wide variety of building types, urban layouts, and geographical variations. Table 1 and Table 2 list the specific city sources, spatial resolutions, and the number of image pairs acquired from public geoportals and commercial providers, respectively.

DSM Data Underutilization: A Critical Gap. Despite the clear advantages of DSMs for detailed building analysis, their use in pre-training remote sensing models remains surprisingly limited. Table 3 presents a comparative analysis of DSM data utilization in various pre-trained remote sensing models. As

Table 1: Aerial Imagery and DSM Data Sources (Public Geoportals).

Country	City/Region	Spatial Resolution (in m)	Number of DSM-RGB Pairs
Germany	Augsburg	0.5	26928
Germany	Berlin	0.5	24186
Germany	Bochum	0.5	1936
Switzerland	Appenzel	0.5	289
Switzerland	Basel	0.5	2300
Switzerland	Bern	0.5	6794
Switzerland	BuchSG	0.5	2288
Switzerland	Geneva	0.5	8108
Switzerland	Herisau	0.5	884
Switzerland	Lausanne	0.5	5355
Switzerland	St. Gallen	0.5	3111
Switzerland	Winterthur	0.5	1352
Switzerland	Zurich	0.5	3172

Table 2: Satellite Imagery and DSM Data Sources (Commercial and Other Sources).

Country	City/Region	Spatial Resolution (in m)	Number of DSM-RGB Pairs
Brazil	São Paulo	0.5	19320
Colombia	Medellin	0.3	1539
Germany	Berlin	0.3	21164
Germany	Dresden	0.2	47526
Germany	Hamburg	0.5	1734
Germany	Juelich	0.5	8066
Germany	Munich	0.5	8712
Germany	North Rhine-Westphalia	0.3-0.5	131224
Libya	Tripoli	0.5	16146
United States	Washington	0.5	2793
Vietnam	Ho Chi Minh City	0.5	143
Jordan	Jordan	0.5	846
Kyrgyzstan	Kyrgyzstan	0.5	15240

the table highlights, most existing models either do not incorporate DSMs or use them in limited quantities, often relying on datasets where DSMs are not the primary focus. This underutilization persists despite evidence suggesting

Table 3: DSM Data Utilization in Pre-trained Remote Sensing Models.

Model	DSM Data Included in Pre-training	Approximate Number of DSM Images in Pre-training Dataset
SatMAE [8]	No	0
RingMo [35]	No	0
GFM [26]	No	0
DeCUR [38]	Yes	6942
SatlasPretrain [3]	No	0
CROMA [12]	No	0
msGFM [17]	Yes	40k
Scale-MAE [28]	No	0
HiRes-FusedMIM (Ours)	Yes	368k

that DSMs can significantly improve performance in tasks such as building segmentation and 3D modeling.

The limited use of DSMs in pre-training underscores the importance and novelty of our approach. By creating a large-scale, high-resolution dataset specifically tailored for RGB-DSM fusion and using it to pre-train HiRes-FusedMIM, our research directly addresses this gap, enabling the development of models that can effectively leverage the rich information contained within DSMs for building-related analysis.

3.2. HiRes-FusedMIM Model Architecture

HiRes-FusedMIM is designed to learn joint representations from paired high-resolution RGB and DSM data, employing a dual encoder architecture based on the SimMIM framework [40]. Figure 1 provides a detailed illustration of the architecture.

Dual Encoders and Decoders. Each encoder branch processes its respective modality—the RGB encoder operates on 3-channel RGB images, while the DSM encoder takes a single-channel DSM. Both encoders are implemented using a Swin transformer architecture [24] to effectively capture local and global image context, which is especially crucial for high-resolution imagery. The model includes two separate decoder branches, one for reconstructing the masked RGB patches and another for reconstructing the masked DSM patches. Each decoder is a lightweight network, designed to map the encoded features back to the original image space.

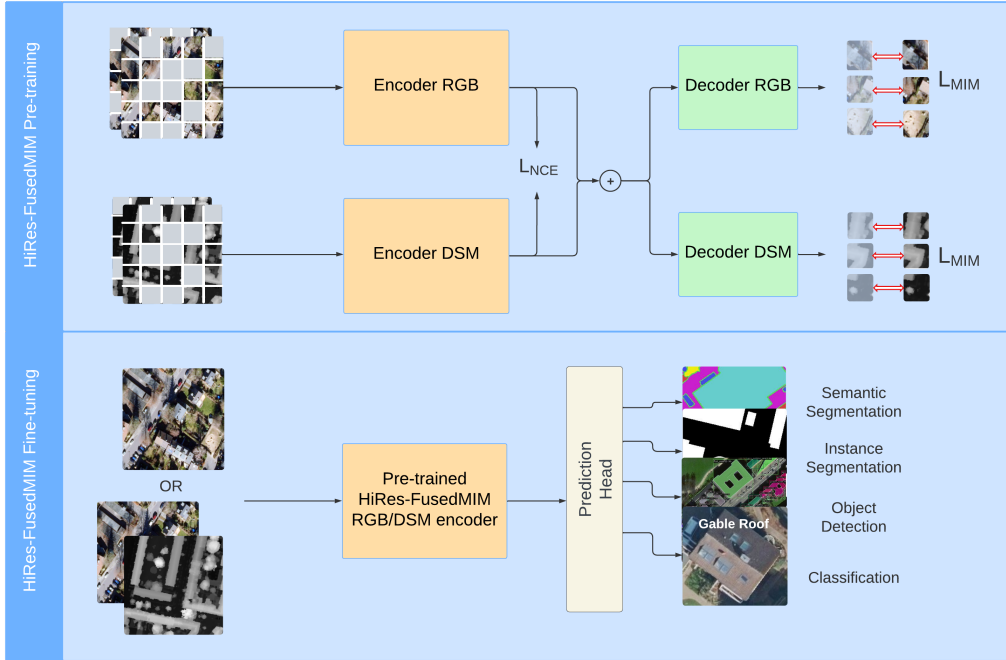


Figure 1: HiRes-Fused pre-training and fine-tuning.

Feature Concatenation. To facilitate cross-modal interaction and the learning of joint representations, the features from the final layer of each encoder are concatenated channel-wise, resulting in a feature vector of dimension of 2048. This concatenated feature vector is then passed to both decoders.

Reconstruction Loss. The decoders are trained to reconstruct the masked patches from their respective modalities, supervised by a reconstruction loss. We employ the L1 loss [40] for this purpose, defined as:

$$\mathcal{L}_{\text{MIM}} = \frac{\|\mathbf{X}_{\text{RGB}} - \mathbf{R}_{\text{RGB}}\|_1 + \|\mathbf{X}_{\text{DSM}} - \mathbf{R}_{\text{DSM}}\|_1}{N}, \quad (1)$$

where \mathbf{X}_{RGB} and \mathbf{X}_{DSM} are original pixel values of masked RGB and DSM patches, respectively. \mathbf{R}_{RGB} and \mathbf{R}_{DSM} are reconstructed pixel values (model outputs) for the RGB and DSM patches, respectively. N is the total number of masked pixels across both RGB and DSM patches.

Contrastive Loss (InfoNCE). To further encourage the alignment of RGB and DSM representations, we introduce a contrastive loss between the out-

put embeddings of the two encoders. We utilize the InfoNCE loss [27], which encourages similar representations for positive pairs (RGB and DSM embeddings from the same location) while pushing dissimilar representations for negative pairs (embeddings from different locations). The InfoNCE loss is defined as:

$$\mathcal{L}_{\text{InfoNCE}} = -\log \left(\frac{\exp(\text{sim}(\mathbf{z}_i, \mathbf{z}_j)/\tau)}{\sum_{k=1}^K \exp(\text{sim}(\mathbf{z}_i, \mathbf{z}_k)/\tau)} \right) \quad (2)$$

where, \mathbf{z}_i and \mathbf{z}_j are the output embeddings from RGB and DSM encoders for a positive pair. τ represents temperature parameter, K represents the number of negative samples and $\text{sim}(\mathbf{z}_i, \mathbf{z}_j)$ is the Cosine similarity between embeddings \mathbf{z}_i and \mathbf{z}_j .

Multi-Objective Loss Function. The total loss function used during pre-training combines the reconstruction losses and the contrastive loss with a weighting factor (α) to balance their contributions:

$$\mathcal{L}_{\text{total}} = (1 - \alpha) * \mathcal{L}_{\text{MIM}} + \alpha * \mathcal{L}_{\text{InfoNCE}} \quad (3)$$

We set $\alpha = 0.05$, allocating 95% of the weight to the MIM objective and 5% to the contrastive loss. This weighting encourages the model to prioritize accurate reconstruction while benefiting from the representation alignment provided by the contrastive loss.

Pre-Training Details. Before pre-training, we performed per-city normalization on the RGB and DSM images. For each city represented in our dataset, we calculated the mean (μ) and standard deviation (σ) values across all RGB channels and DSM channel. Each image (I) from that city was then normalized using the following equation:

$$I_{\text{normalized}} = \frac{I - \mu}{\sigma} \quad (4)$$

This normalization helps mitigate variations in illumination, atmospheric conditions, and sensor characteristics across different sources.

During pre-training, we randomly masked 60% of the input patches in each training iteration, a strategy consistent with findings that suggest larger

masking ratios can lead to improved performance [26, 40]. We augmented the training data with random horizontal flipping and random cropping to encourage the model to learn more robust representations. The AdamW optimizer [23] was used with a base learning rate of 5e-4 and a cosine learning rate schedule. The model was trained for 400 epochs with a batch size of 128 per GPU on 8 NVIDIA V100 GPUs and an image size of 224×224 .

4. Experiments and Results

This section presents a comprehensive evaluation of HiRes-FusedMIM, highlighting its effectiveness in learning powerful representations from high-resolution RGB-DSM data for building-related tasks. We first demonstrate the reconstruction capabilities of the model after pre-training, visually highlighting its ability to capture intricate details from both modalities. We then analyze the performance of the model on various downstream tasks, comparing it to relevant baselines and existing foundation models.

4.1. Pre-Training Evaluation: Qualitative Analysis of Reconstructions

Figure 2 showcases the ability of HiRes-FusedMIM to reconstruct masked patches from both RGB and DSM inputs after pre-training. The figure presents examples of input images with masked regions, the corresponding reconstructed outputs, and the original unmasked images.

As evident from the visualizations in Figure 2, HiRes-FusedMIM achieves impressive reconstruction quality for both RGB and DSM data. The model accurately recovers fine details, such as building edges, roof structures, and subtle variations in elevation, indicating its ability to learn meaningful representations of the underlying spatial structures and cross-modal relationships. These strong reconstruction capabilities suggest that the pre-trained model has acquired valuable knowledge that can be effectively leveraged for downstream tasks requiring detailed building information.

4.2. Image Classification

We evaluated HiRes-FusedMIM on two widely used classification benchmarks: the UC Merced Land Use Dataset (UCM) and the BigEarthNet (BEN) dataset. UCM, with its 21 land-use classes and relatively high resolution (0.3m), allows us to assess the performance of the model on data similar in resolution to the pre-training data. BEN, a multi-label classification dataset with 12-band Sentinel-2 imagery at 10m, 20m, and 60m resolutions,

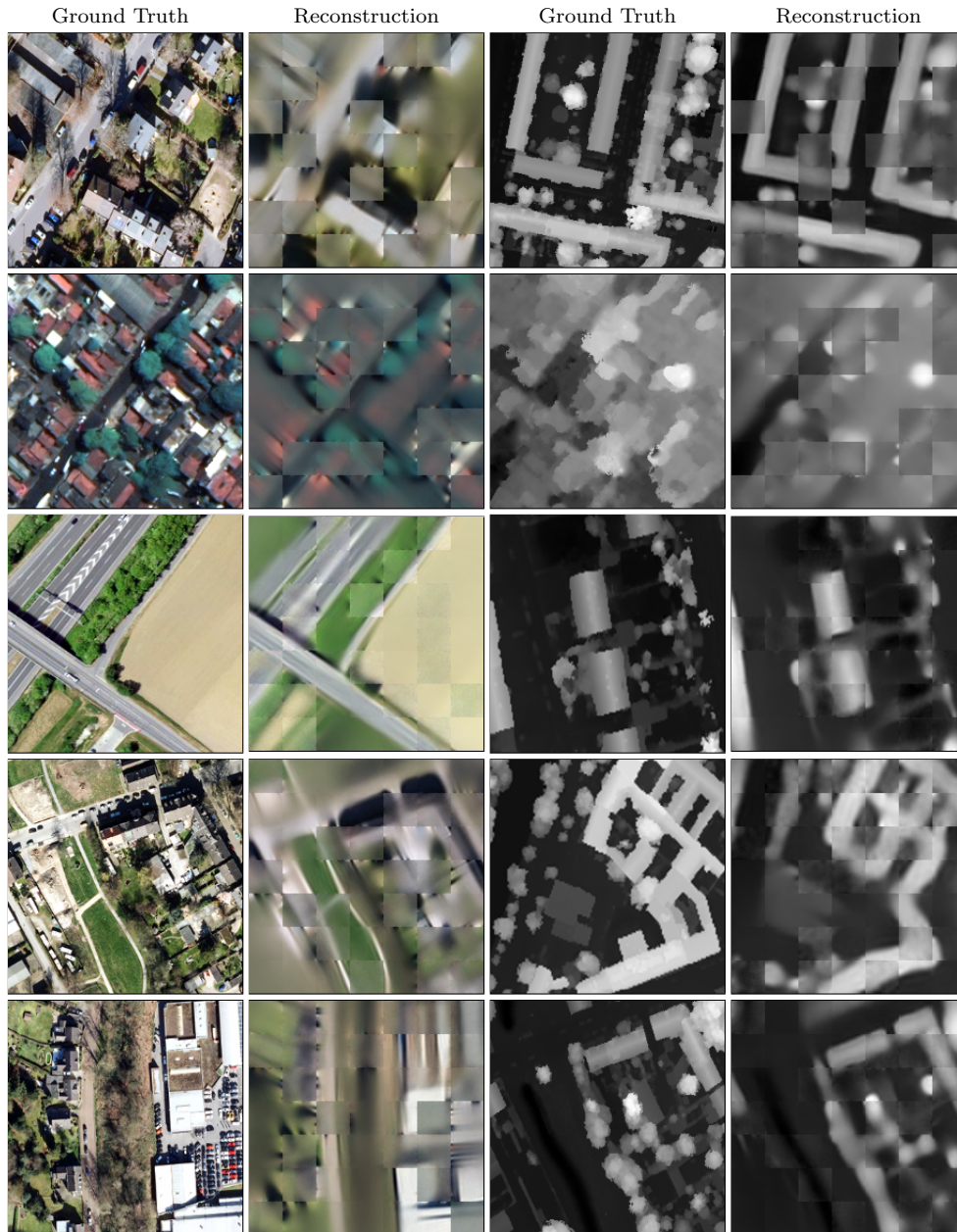


Figure 2: Visualization of the reconstruction capabilities of the pretrained model. The left two columns represent ground truth and reconstructions from RGB samples, while the right two columns depict ground truth and reconstructions from DSM samples.

Table 4: UC Merced classification accuracy and BigEarthNet multi-label classification mean average precision results.

Method	UCM	BEN 1%	BEN 10%
ResNet50 (ImageNet-1k) [19]	98.8	41.3	80.0
SeCo [25]	97.1	63.6	82.6
ViT (ImageNet-22k) [10]	93.1	73.6	84.7
SatMAE [8]	92.6	68.9	81.8
Swin-B (random) [24]	66.9	65.7	80.6
Swin-B (ImageNet-22k) [24]	99.0	79.5	85.7
GFM [26]	99.0	80.7	86.3
HiRes-FusedMIM	98.1	75.9	84.7

enables us to analyze generalization capabilities of the model when it is applied to lower-resolution data. We followed the same classification pipeline as described in [26], utilizing Swin-Base transformer with a linear classifier head.

Table 4 presents the classification accuracy of HiRes-FusedMIM on the UCM and BEN datasets. Note that the results for other models were obtained from their respective publications and are provided here for context and comparison with our proposed approach. We have not reproduced these algorithms at our end. While not achieving state-of-the-art results, HiRes-FusedMIM demonstrates strong performance, achieving 98.1% accuracy on UCM and 84.7% mean average precision (mAP) on BEN (10% data). These results are particularly encouraging considering the relatively small size of our pre-training dataset (around 368k images) compared to the larger datasets used by top-performing models like GFM (600k images). This suggests that our focus on curating a high-quality, high-resolution, and multi-modal dataset can lead to competitive performance even with a more compact training set. Furthermore, on the BigEarthNet dataset, which uses lower-resolution Sentinel-2 imagery, HiRes-FusedMIM outperforms other foundation models like SeCo and SatMAE, both of which are pre-trained solely on Sentinel-2 data. Our findings align with the observations in [34], where models pre-trained on higher-resolution data exhibited an advantage in classifying lower-resolution imagery. This highlights the potential of HiRes-FusedMIM to generalize effectively across different spatial resolutions, making it suitable for a wider range of remote sensing applications.

4.3. Semantic Segmentation

To evaluate the effectiveness of HiRes-FusedMIM for semantic segmentation, we conducted experiments on five datasets:

- WHU Aerial Building Dataset [22]: A high-resolution (0.3 m GSD) dataset for building segmentation, where we evaluated the RGB encoder of HiRes-FusedMIM.
- LoveDA Dataset [37]: A domain adaptation dataset (0.3 m resolution) featuring seven land cover classes. The dataset encompasses both urban and rural domains, which brings considerable challenges due to the: 1) multi-scale objects; 2) complex background samples; and 3) inconsistent class distributions.
- Vaihingen Dataset [29]: A benchmark dataset with both RGB and DSM data (0.9 m resolution), enabling assessment of multi-modal learning capabilities. We evaluate both the RGB and the combined RGB-DSM encoders of HiRes-FusedMIM.
- GeoNRW Dataset [2]: This dataset provides a diverse set of urban scenes, including orthorectified aerial photographs, LiDAR-derived digital elevation models (DEMs), and OpenStreetMap-refined segmentation maps. It covers 10 classes and features data from the German state of North Rhine-Westphalia. The dataset is particularly relevant for our work, as it allows us to assess the performance of HiRes-FusedMIM on both RGB and DSM modalities.
- SpaceNet Building Detection Dataset (V1) [11]: A large-scale dataset with high-resolution (0.5 m) imagery for building footprint extraction.

We employed a encoder-decoder architecture with a Swin-Base transformer backbone [24] for all semantic segmentation tasks. For Vaihingen and GeoNRW, which provide both RGB and DSM data, we designed a Dual-SwinTransformer backbone, incorporating two separate Swin Transformers - one for RGB input and another for DSM input. We chose UPerNet [39] from the MMSegmentation library [9] as the architecture of the decoder for all the datasets.

We trained all models for 40k iterations with an input image size of 512×512 , using the Adam optimizer and the default learning rate of $1e-4$. All training settings were consistent with the default configuration in MMSegmentation.



Figure 3: HiRes-FusedMIM Demonstrates Accurate Segmentation of Buildings and Other Urban Features: Visualized Results on Whu Aerial, LoveDA, Vaihingen, GeoNRW, and SpaceNetv1 datasets.

Table 5: Results for semantic segmentation datasets with RGB modality.

Method	Backbone	WHU Aerial	LoveDA	Vaihingen	SpaceNetV1
SeCo	ResNet-50	86.7	43.63	68.9	73.89
GeoKR	VGG-16	-	-	74.01	-
GASSL	ResNet-50	-	48.76	-	78.51
SatMAE	ViT-L	82.5	-	70.6	78.07
UperNet(random)	Swin-B	88.2	44.24	67.0	-
GFM	Swin-B	90.7	-	75.3	72.81
CMID	Swin-B	-	-	-	65.98
CtxMIM	Swin-B	-	-	-	79.22
MAE + MTP	ViT-B + RVSA	-	52.39	-	79.63
BillionFM	ViT-L12×4	-	52.38	-	-
HiRes-FusedMIM	Swin-B	91.28	52.54	74.16	78.37

Table 5 presents the quantitative results (mIoU) for HiRes-FusedMIM on the RGB-only datasets. For comparison, we include results from other foundation models and baseline approaches. Note that the results for other models were obtained from their respective publications and are provided here to contextualize the performance of our proposed approach.

Table 6 compares the performance of three different model configurations on the Vaihingen and GeoNRW datasets: 1) a U-Net with randomly initialized Swin-Base encoder and UPerNet decoder trained in a supervised fashion, 2) the same U-Net architecture but with the encoder initialized using the weights from the HiRes-FusedMIM RGB encoder, and 3) a U-Net with the DualSwinTransformer backbone, where both the RGB and DSM encoders are initialized with the corresponding weights from HiRes-FusedMIM.

HiRes-FusedMIM demonstrates excellent performance on both the WHU Aerial and LoveDA datasets, achieving state-of-the-art results and surpassing existing pre-trained models and supervised baselines. On the Vaihingen and SpaceNet datasets, our model achieves mIoU scores that are comparable to other high-performing methods, showcasing its effectiveness across various datasets and for tasks requiring detailed building information. The results on the Vaihingen and GeoNRW datasets, which include DSM data, further emphasize the benefits of multi-modal learning. On Vaihingen, initializing the U-Net encoder with weights from the HiRes-FusedMIM RGB encoder yields a 74.16% mIoU, significantly outperforming the randomly initialized model (65.28% mIoU). Incorporating the DSM modality and initializing both encoders with the corresponding HiRes-FusedMIM weights results in a further improvement, achieving a 74.4% mIoU. Similar trends are observed on the

Table 6: Results for semantic segmentation task datasets with RGB and DSM modality.

Method	Modality	Vaihingen	GeoNRW
Supervised (Swin-B)	RGB	65.28	54.8
HiRes-FusedMIM	RGB	74.16	59.39
HiRes-FusedMIM	RGB+DEM/DSM	74.4	61.68

GeoNRW dataset, where adding the DSM modality leads to a notable boost in performance (61.68% mIoU compared to 59.39% with only RGB). These findings highlight the effectiveness of HiRes-FusedMIM in leveraging both RGB and DSM data to improve segmentation accuracy in complex urban environments.

4.4. Instance Segmentation

To assess the effectiveness of HiRes-FusedMIM for instance segmentation, we conducted experiments using the UBCv2 dataset [20], a benchmark designed for building detection and fine-grained classification from very high-resolution (VHR) satellite imagery. The dataset comprises annotated polygons for approximately 0.5 million building instances across 12 roof types, encompassing VHR optical images from 20 diverse cities worldwide, showcasing a wide array of architectural styles and landforms. Seventeen of these cities are also provided with aligned synthetic aperture radar (SAR) imagery, facilitating the development and evaluation of approaches optionally utilizing optical, SAR, or combined modalities. We focused on evaluating the performance of our RGB encoder weights using only the optical imagery from UBCv2.

We employed the Mask R-CNN model [18], a widely used architecture for instance segmentation, with a Swin Transformer backbone [24] from the MMDetection library [7]. We compared our approach to several baselines, including randomly initialized and ImageNet pre-trained Mask R-CNN models, as well as variants utilizing more complex techniques such as Cascade Mask R-CNN with a class-wise geometric transformer (CGT) module introduced in [20]. These baseline results, obtained from [20], showcase the performance achieved using a ResNet backbone [19] for the Mask R-CNN model. In our experiments, we first replaced the ResNet backbone with a randomly initialized Swin-Base [24] transformer to establish a baseline performance for this backbone. We then initialized the Swin-Base backbone with weights from



Figure 4: HiRes-FusedMIM Effectively Segments Individual Buildings in Diverse Urban Environments: Visualized Examples from the UBCv2 Test Set.

Table 7: Instance segmentation results using AP (%) on UBCv2 Test set with Fine-Grained roof classes: FL-Flat, GA-Gable, GM-Gambrel, RO- Row, ME- Multiple Eave, H1- Hipped V1, H2- Hipped V2, MA- Mansard, PY- Pyramid, AR-Arched, RE- Revolved and OT-Other.

Method	AP	AP_{50}	FL	GA	GM	RO	ME	H1	H2	MA	PY	AR	RE	OT
SOLOv2	14.2	24.0	24.6	21.3	27.7	5.8	9.5	7.6	35.0	3.6	4.6	14.8	11.2	6.1
QueryInst	15.3	25.2	25.5	23.4	28.6	5.1	24.2	8.9	33.9	7.0	4.8	13.9	4.5	5.5
Mask R-CNN	15.5	25.9	25.8	24.7	29.2	5.1	12.3	10.0	39.0	5.4	5.6	16.8	5.8	7.2
Cascade Mask R-CNN	16.5	26.9	26.5	24.5	29.1	4.7	19.7	10.9	38.6	6.0	7.0	18.5	6.7	6.4
Mask R-CNN + CGT	16.3	26.3	25.2	25.1	27.4	9.0	21.6	9.8	39.6	5.7	5.8	17.2	3.2	6.8
Cascade Mask R-CNN + CGT	17.1	27.1	27.2	25.0	28.6	6.6	24.9	11.1	39.8	7.7	5.8	16.4	5.7	7.2
Mask R-CNN (SWIN-B)	14.8	24.5	43.8	40.8	49.4	4.3	30.2	8.7	47.2	6.7	7.7	13.3	30.5	11.7
HiRes-FusedMIM	17.7	28.5	47.32	45.4	54.9	13.7	27.8	16.1	59.0	12.6	12.7	20.9	18.6	12.4

the RGB encoder of HiRes-FusedMIM to evaluate the transferability of the learned representations.

Table 7 presents the instance segmentation results on the UBCv2 test set, using Average Precision (AP) and AP_{50} as evaluation metrics. Notably, our experiments revealed that the Mask R-CNN model with a randomly initialized Swin-Base backbone (14.8% AP) performs less effectively compared to the ResNet-based counterparts reported in the [20]. However, initializing the Swin-Base backbone with weights from our pre-trained HiRes-FusedMIM RGB encoder leads to a substantial improvement, achieving an 17.7% AP, surpassing all baseline models, including the top-performing Cascade Mask R-CNN + CGT model (17.1% AP), by a significant margin. This highlights the effectiveness of our pre-training strategy in learning robust and generalizable representations that transfer well to instance segmentation, even when utilizing a different backbone architecture.

5. Ablation Studies

To gain a deeper understanding of the contributions of different components within HiRes-FusedMIM, we conducted a series of ablation studies. These studies analyze the impact of the DSM encoder and the contrastive loss component.

5.1. Impact of DSM Encoder

To assess the contribution of the DSM encoder, we compared the performance of HiRes-FusedMIM with and without the DSM modality on datasets that provide both RGB and DSM data (Vaihingen and GeoNRW). As shown in Table 6, incorporating the DSM data consistently leads to a performance

Table 8: Impact of Contrastive Loss on Downstream Task Performance

Method	UCM	BEN		WHU	LoveDA	Vaihingen		GeoNRW		SpaceNetV1	UBCv2	
		1%	10%			RGB	RGB+DSM	RGB	RGB+DSM		AP	AP ₅₀
MIM	96.7	76.1	84.68	91.13	52.35	73.84	73.1	58.9	61.13	78.32	16.9	27.4
MIM+Contrastive	98.1	76.9	85.1	91.28	52.54	74.16	74.4	59.39	61.68	78.37	17.7	28.5

improvement. On the Vaihingen dataset, adding the DSM encoder and initializing it with the corresponding HiRes-FusedMIM weights increases the mIoU from 74.16% (RGB-only) to 74.4%. Similarly, on the GeoNRW dataset, the mIoU increases from 59.39% (RGB-only) to 61.68% with the inclusion of the DSM modality. These results clearly demonstrate the value of incorporating DSM data and training a dedicated DSM encoder for tasks involving building-level analysis. The DSM encoder enables the model to capture fine-grained elevation information and to learn richer, multi-modal representations, leading to more accurate segmentation results.

5.2. Impact of Contrastive Loss

We investigated the contribution of the contrastive loss component (InfoNCE loss) in the multi-objective loss function used to pre-train HiRes-FusedMIM. We compared two versions of the model:

- HiRes-FusedMIM (MIM+Contrastive): The full model, pre-trained with both the reconstruction loss (\mathcal{L}_{MIM}) and the contrastive loss ($\mathcal{L}_{\text{InfoNCE}}$), as described in section 3.
- HiRes-FusedMIM (MIM): A variant of the model trained solely with the reconstruction loss (\mathcal{L}_{MIM}), excluding the contrastive loss.

Table 8 presents the quantitative results of both models across all downstream tasks.

As shown in Table 8, incorporating the contrastive loss during pre-training consistently leads to improved performance across most downstream tasks. While the gains are relatively small on some tasks, we observe more significant improvements on Vaihingen (RGB+DSM), GeoNRW (RGB+DSM), and UBCv2. This suggests that the contrastive loss is particularly beneficial for tasks that rely heavily on the integration of RGB and DSM information. By encouraging the encoders to learn aligned representations for both modalities, the contrastive loss facilitates more effective multi-modal fusion, leading to superior performance on these tasks.

6. Conclusion

This paper presented *HiRes-FusedMIM*, a novel pre-trained model specifically designed for building-level analysis in remote sensing. Recognizing the under-utilization of high-resolution digital surface models (DSMs) in existing pre-trained models, we explored the benefits of integrating DSM data with RGB imagery. Our approach involved:

- Curating a large-scale, high-resolution dataset: We created a unique dataset of over 368k paired RGB-DSM image pairs at a resolution of 0.2-0.5 m, meticulously gathered from various sources across Europe.
- Designing a dual-encoder SimMIM architecture: Our model utilizes separate encoders for processing RGB and DSM data, allowing for specialized feature learning tailored to each modality. This dual-encoder design is further enhanced by incorporating a contrastive loss (InfoNCE) to promote alignment between the learned representations.
- Extensive evaluation on diverse downstream tasks: We evaluated HiRes-FusedMIM on a wide range of building-related tasks, including classification, semantic segmentation, and instance segmentation, demonstrating its ability to effectively capture and leverage fine-grained, multi-modal information.

Our experiments showcase that incorporating DSM data during pre-training consistently leads to improved performance, particularly on tasks involving building extraction and segmentation. HiRes-FusedMIM achieves best results among its peer models on datasets like WHU Aerial and LoveDA, highlighting its effectiveness in learning robust and generalizable representations for building-focused analysis. Furthermore, our ablation studies confirm the advantages of our dual-encoder architecture and the contribution of the contrastive loss in enhancing multi-modal fusion.

The development of HiRes-FusedMIM highlights the potential of leveraging high-resolution DSM data for pre-training in remote sensing. By sharing our pre-trained model weights, we aim to facilitate further research and applications in this direction, encouraging the community to explore the benefits of multi-modal learning for building-level analysis.

This research has demonstrated the effectiveness of pre-training with high-resolution RGB-DSM data for building-level analysis. Building upon

these findings, several promising research avenues exist for further exploration. We plan to investigate the application of HiRes-FusedMIM to tasks such as DSM to DTM generation and building height prediction, leveraging its ability to capture detailed elevation information and learn multi-modal representations. Additionally, we aim to explore the potential of using the strong embeddings from the model within a 3D building reconstruction pipeline, potentially leading to more accurate and efficient reconstruction methods. Further investigation is needed to optimize the fusion techniques and fine-tuning strategies for these tasks, ensuring that the benefits of HiRes-FusedMIM are fully realized.

References

- [1] Bachmann, R., Mizrahi, D., Atanov, A., Zamir, A., 2022. Multimaes: Multi-modal multi-task masked autoencoders.
- [2] Baier, G., Deschemps, A., Schmitt, M., Yokoya, N., 2020. Geonrw.
- [3] Bastani, F., Wolters, P., Gupta, R., Ferdinando, J., Kembhavi, A., 2023. Satlaspretrain: A large-scale dataset for remote sensing image understanding, in: 2023 IEEE/CVF International Conference on Computer Vision (ICCV), pp. 16726–16736.
- [4] Bittner, K., Adam, F., Cui, S., Körner, M., Reinartz, P., 2018. Building footprint extraction from vhr remote sensing images combined with normalized dsms using fused fully convolutional networks. *IEEE Journal of Selected Topics in Applied Earth Observations and Remote Sensing* 11, 2615–2629.
- [5] Bittner, K., Reinartz, P., Körner, M., 2019. Late or earlier information fusion from depth and spectral data? large-scale digital surface model refinement by hybrid-cgan, in: 2019 IEEE/CVF Conference on Computer Vision and Pattern Recognition Workshops (CVPRW), pp. 1471–1478.
- [6] Cha, K., Seo, J., Lee, T., 2024. A billion-scale foundation model for remote sensing images. *IEEE Journal of Selected Topics in Applied Earth Observations and Remote Sensing* , 1–17.

- [7] Chen, K., Wang, J., Pang, J., Cao, Y., Xiong, Y., Li, X., Sun, S., Feng, W., Liu, Z., Xu, J., Zhang, Z., Cheng, D., Zhu, C., Cheng, T., Zhao, Q., Li, B., Lu, X., Zhu, R., Wu, Y., Dai, J., Wang, J., Shi, J., Ouyang, W., Loy, C.C., Lin, D., 2019. MMDetection: Open mmlab detection toolbox and benchmark. arXiv preprint arXiv:1906.07155 .
- [8] Cong, Y., Khanna, S., Meng, C., Liu, P., Rozi, E., He, Y., Burke, M., Lobell, D.B., Ermon, S., 2023. Satmae: Pre-training transformers for temporal and multi-spectral satellite imagery .
- [9] Contributors, M., 2020. MMSegmentation: Openmmlab semantic segmentation toolbox and benchmark.
- [10] Dosovitskiy, A., Beyer, L., Kolesnikov, A., Weissenborn, D., Zhai, X., Unterthiner, T., Dehghani, M., Minderer, M., Heigold, G., Gelly, S., Uszkoreit, J., Houlsby, N., 2021. An image is worth 16x16 words: Transformers for image recognition at scale.
- [11] Etten, A.V., Lindenbaum, D., Bacastow, T.M., 2019. Spacenet: A remote sensing dataset and challenge series.
- [12] Fuller, A., Millard, K., Green, J.R., 2023. Croma: Remote sensing representations with contrastive radar-optical masked autoencoders.
- [13] Gui, J., Chen, T., Zhang, J., Cao, Q., Sun, Z., Luo, H., Tao, D., 2024a. A survey on self-supervised learning: Algorithms, applications, and future trends. *IEEE Transactions on Pattern Analysis and Machine Intelligence* , 1–20.
- [14] Gui, S., Qin, R., 2021. Automated lod-2 model reconstruction from very-high-resolution satellite-derived digital surface model and orthophoto. *ISPRS Journal of Photogrammetry and Remote Sensing* 181, 1–19.
- [15] Gui, S., Schuegraf, P., Bittner, K., Qin, R., 2024b. Unit-level lod2 building reconstruction from satellite-derived digital surface model and orthophoto. *ISPRS Annals of the Photogrammetry, Remote Sensing and Spatial Information Sciences X-2-2024*, 81–88.
- [16] Guo, X., Lao, J., Dang, B., Zhang, Y., Yu, L., Ru, L., Zhong, L., Huang, Z., Wu, K., Hu, D., He, H., Wang, J., Chen, J., Yang, M., Zhang, Y., Li, Y., 2024. Skysense: A multi-modal remote sensing foundation model

- towards universal interpretation for earth observation imagery, in: 2024 IEEE/CVF Conference on Computer Vision and Pattern Recognition (CVPR), pp. 27662–27673.
- [17] Han, B., Zhang, S., Shi, X., Reichstein, M., 2024. Bridging remote sensors with multisensor geospatial foundation models, in: 2024 IEEE/CVF Conference on Computer Vision and Pattern Recognition (CVPR), pp. 27852–27862.
- [18] He, K., Gkioxari, G., Dollár, P., Girshick, R., 2018. Mask r-cnn.
- [19] He, K., Zhang, X., Ren, S., Sun, J., 2015. Deep residual learning for image recognition.
- [20] Huang, X., Chen, K., Tang, D., Liu, C., Ren, L., Sun, Z., Hänsch, R., Schmitt, M., Sun, X., Huang, H., Mayer, H., 2023. Urban building classification (ubc) v2—a benchmark for global building detection and fine-grained classification from satellite imagery. *IEEE Transactions on Geoscience and Remote Sensing* 61, 1–16.
- [21] Jakubik, J., Roy, S., Phillips, C.E., Fraccaro, P., Godwin, D., Zadrozny, B., Szwarcman, D., Gomes, C., Nyirjesy, G., Edwards, B., Kimura, D., Simumba, N., Chu, L., Mukkavilli, S.K., Lambhate, D., Das, K., Bangalore, R., Oliveira, D., Muszynski, M., Ankur, K., Ramasubramanian, M., Gurung, I., Khallaghi, S., Hanxi, Li, Cecil, M., Ahmadi, M., Kordi, F., Alemohammad, H., Maskey, M., Ganti, R., Weldemariam, K., Ramachandran, R., 2023. Foundation models for generalist geospatial artificial intelligence .
- [22] Ji, S., Wei, S., Lu, M., 2019. Fully convolutional networks for multi-source building extraction from an open aerial and satellite imagery data set. *IEEE Transactions on Geoscience and Remote Sensing* 57, 574–586.
- [23] Kingma, D.P., Ba, J., 2017. Adam: A method for stochastic optimization.
- [24] Liu, Z., Lin, Y., Cao, Y., Hu, H., Wei, Y., Zhang, Z., Lin, S., Guo, B., 2021. Swin transformer: Hierarchical vision transformer using shifted windows, in: 2021 IEEE/CVF International Conference on Computer Vision (ICCV), pp. 9992–10002.

- [25] Mañas, O., Lacoste, A., Giró-i Nieto, X., Vazquez, D., Rodríguez, P., 2021. Seasonal contrast: Unsupervised pre-training from uncurated remote sensing data, in: 2021 IEEE/CVF International Conference on Computer Vision (ICCV), pp. 9394–9403.
- [26] Mendieta, M., Han, B., Shi, X., Zhu, Y., Chen, C., 2023. Towards geospatial foundation models via continual pretraining, in: 2023 IEEE/CVF International Conference on Computer Vision (ICCV), pp. 16760–16770.
- [27] van den Oord, A., Li, Y., Vinyals, O., 2019. Representation learning with contrastive predictive coding.
- [28] Reed, C.J., Gupta, R., Li, S., Brockman, S., Funk, C., Clipp, B., Keutzer, K., Candido, S., Uyttendaele, M., Darrell, T., 2023. Scale-mae: A scale-aware masked autoencoder for multiscale geospatial representation learning, in: 2023 IEEE/CVF International Conference on Computer Vision (ICCV), pp. 4065–4076.
- [29] Rottensteiner, F., Sohn, G., Jung, J., Gerke, M., Baillard, C., Benitez, S., Breitkopf, U., 2012. The isprs benchmark on urban object classification and 3d building reconstruction. ISPRS Annals of the Photogrammetry, Remote Sensing and Spatial Information Sciences I-3, 293–298.
- [30] Schuegraf, P., Bittner, K., 2019. Automatic building footprint extraction from multi-resolution remote sensing images using a hybrid fcn. ISPRS International Journal of Geo-Information 8.
- [31] Schuegraf, P., Shan, J., Bittner, K., 2024a. Planes4lod2: Reconstruction of lod-2 building models using a depth attention-based fully convolutional neural network. ISPRS Journal of Photogrammetry and Remote Sensing 211, 425–437.
- [32] Schuegraf, P., Stiller, D., Tian, J., Stark, T., Wurm, M., Taubenböck, H., Bittner, K., 2024b. Ai-based building instance segmentation in formal and informal settlements, in: IGARSS 2024 - 2024 IEEE International Geoscience and Remote Sensing Symposium, pp. 1558–1561.
- [33] Schuegraf, P., Zorzi, S., Fraundorfer, F., Bittner, K., 2023. Deep learning for the automatic division of building constructions into sections on

- remote sensing images. *IEEE Journal of Selected Topics in Applied Earth Observations and Remote Sensing* 16, 7186–7200.
- [34] Stojnić, V., Risojević, V., 2021. Self-supervised learning of remote sensing scene representations using contrastive multiview coding, in: 2021 IEEE/CVF Conference on Computer Vision and Pattern Recognition Workshops (CVPRW), pp. 1182–1191.
- [35] Sun, X., Wang, P., Lu, W., Zhu, Z., Lu, X., He, Q., Li, J., Rong, X., Yang, Z., Chang, H., He, Q., Yang, G., Wang, R., Lu, J., Fu, K., 2023. Ringmo: A remote sensing foundation model with masked image modeling. *IEEE Transactions on Geoscience and Remote Sensing* 61, 1–22.
- [36] Tack, F., Buyuksalih, G., Goossens, R., 2012. 3d building reconstruction based on given ground plan information and surface models extracted from spaceborne imagery. *ISPRS Journal of Photogrammetry and Remote Sensing* 67, 52–64.
- [37] Wang, J., Zheng, Z., Ma, A., Lu, X., Zhong, Y., 2022. Loveda: A remote sensing land-cover dataset for domain adaptive semantic segmentation.
- [38] Wang, Y., Albrecht, C.M., Braham, N.A.A., Liu, C., Xiong, Z., Zhu, X.X., 2024. Decoupling common and unique representations for multi-modal self-supervised learning.
- [39] Xiao, T., Liu, Y., Zhou, B., Jiang, Y., Sun, J., 2018. Unified perceptual parsing for scene understanding.
- [40] Xie, Z., Zhang, Z., Cao, Y., Lin, Y., Bao, J., Yao, Z., Dai, Q., Hu, H., 2022. Simmim: a simple framework for masked image modeling, in: 2022 IEEE/CVF Conference on Computer Vision and Pattern Recognition (CVPR), pp. 9643–9653.
- [41] Xu, Y., Jubanski, J., Bittner, K., Siegert, F., 2024. Roof plane parsing towards lod-2.2 building reconstruction based on joint learning using remote sensing images. *International Journal of Applied Earth Observation and Geoinformation* 133, 104096.